NONLINEAR DYNAMIC SIMULATION OF COUPLED LATERAL-TORSIONAL VIBRATIONS OF A GEAR TRANSMISSION SYSTEM

Shaobin Li[1], Hong-Zhong Huang[2,*] , Xianfeng Fan[2], Qiang Miao[2]

1. Department of Arts Design, Chongqing Normal University, Chongqing, 400047, China
2. School of Mechatronics Engineering, University of Electronic Science and Technology of China, No.4 Section 2 Jianshe North Road, Chengdu, Sichuan, 610054, China

Abstract: Nonlinear dynamic model of the coupled lateral-torsional vibrations of a gear transmission system is developed, in which time-varying gear meshing stiffness, errors, and gaps are considered. The fundamental rules of the system's multi-harmonic dynamic response have been obtained based on the time domain diagram, frequency domain diagram, phase plot, and Poincaré map. Therefore, estimation of the dynamic response can be realized in the period of the system design.

Key words: Nonlinear dynamics simulation; Gear; Vibration; Chaos

1. Introduction

A gear transmission system includes the gears, drafts, and bearings. As an elastic mechanical system, it will generate dynamic response under the dynamic exciting forces. Because of the gaps between the meshing teeth, the multi-impact phenomena of the gear teeth contacting-separating-contacting will occur in the high-speed and starting frequently system [1]. The research of gear transmission system gap nonlinear dynamics has been a focus recently [2]. Considering the urges of stiffness, errors, and meshing impact and adopting the gear transmission system coupled lateral-torsional model, the work in this paper carries out nonlinear dynamics simulation and reaches some beneficial conclusions that will be helpful to the design of gear transmission systems.

2. Establishment of the gear transmission system nonlinear dynamics model

Suppose the stiffness of a nonlinear element is a two-segment symmetrical type. The ration of these two segments' stiffness is 0. Energy consumption element is a linear viscous damper. The fluctuation of the load is neglected. The influence of the inner excitation is considered only. The error impulse generated by the comprehensive meshing error is taken as a simple harmonic function. The meshing stiffness is time-varying. Its average and base frequency components are considered only.

The gear transmission system dynamics model established by centralized quality method is shown in Fig.1, in which, stiffness and damping of the transmission shaft and supporting bearings are expressed with combination equivalent value $k_{1x}, c_{1x}, k_{1y}, c_{1y}, k_{2x}, c_{2x}, k_{2y}$, and c_{2y}; the tooth gaps

are represented as 2*b*; the meshing stiffness is $k(t)$; the damping coefficient is *c*; the error is denoted by $e(t)$; the basic radius of the initiative and passive

Therefore, the dynamic transmission error is

$$y_d(t) = y_1 + r_1\theta_1(t) - y_2 - r_2\theta_2(t). \quad (1)$$

The difference between the dynamic transmission error $y_d(t)$ and the static transmission error $e(t)$ is $y(t)$, given as Eq. (2).

$$y(t) = y_1 + r_1\theta_1(t) - y_2 - r_2\theta_2(t) - e(t). \quad (2)$$

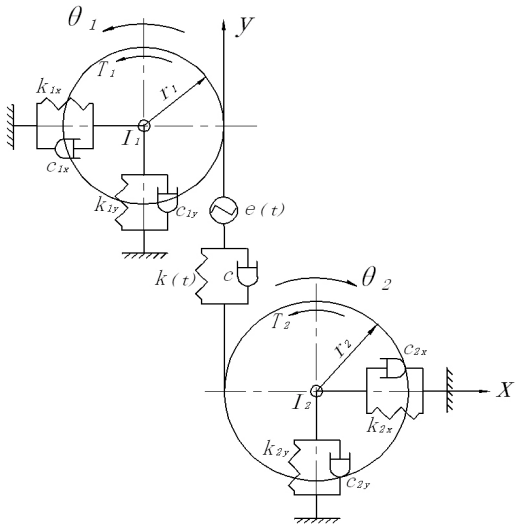

Fig. 1 The gears nonlinear dynamics model

The meshing force is

$$F_y = k(t)f(y) + c\dot{y}(t), \quad (3)$$

where, $f(y)$ is a nonlinear function to describe the meshing force generated by gears with gaps. Since each gap is assumed as symmetrical type, $f(y)$ should be

gears are r_1, r_2, respectively; the torsion angular displacement of the initiative and passive gears are θ_1, θ_2, respectively.

$$f(y) = \begin{cases} y - b & y > b, \\ 0 & |y| \le b, \\ y + b & y < -b. \end{cases} \quad (4)$$

The friction force of the tooth surface can be showed approximately as

$$F_x = \pm\mu F_y, \quad (5)$$

where, μ is the equivalent friction coefficient; F_x is positive along positive *x* direction, otherwise it is negative.

Therefore, the dynamics differential equations of the system can be simplified represented as

$$\begin{cases} m_1\ddot{x}_1 + c_{1x}\dot{x}_1 - \mu c\dot{y} + k_{1x}x_1 - \mu k(t)f(y) = 0 \\ m_1\ddot{y}_1 + c_{1y}\dot{y}_1 + c\dot{y} + k_{1y}y_1 + k(t)f(y) = 0 \\ m_2\ddot{x}_2 + c_{2x}\dot{x}_2 + \mu c\dot{y} + k_{2x}x_2 + \mu k(t)f(y) = 0 \\ m_2\ddot{y}_2 + c_{2y}\dot{y}_2 - c\dot{y} + k_{2y}y_2 - k(t)f(y) = 0 \\ m\ddot{y} - m\ddot{y}_1 + m\ddot{y}_2 + c\dot{y} + k(t)f(y) = F \end{cases}, \quad (6)$$

$$\begin{cases} m = \dfrac{1}{-\dfrac{r_1R_1}{I_1} - \dfrac{r_2R_2}{I_2} + \dfrac{r_1^2}{I_1} + \dfrac{r_2^2}{I_2}} \\ R_1 = \mu(r_1 tg\beta - H) \\ R_2 = \mu(r_2 tg\beta + H) \\ F = F_m - m\ddot{e} = m\left(\dfrac{r_1T_1}{I_1} + \dfrac{r_2T_2}{I_2}\right) - m\ddot{e} \end{cases}, \quad (7)$$

where, m_1, m_2, I_1, and I_2 are the equivalent qualities and the turning inertias of the driving and passive gears, respectively; T_1, T_2 are the input and export torques acting on the driving and passive gears, respectively; β is the meshing angle; *H* is the distance between the meshing point and the pitch point. Eq. (6) can be re-written in the following matrix form

$$\begin{bmatrix} m_1 & 0 & 0 & 0 & 0 \\ 0 & m_1 & 0 & 0 & 0 \\ 0 & 0 & m_2 & 0 & 0 \\ 0 & 0 & 0 & m_2 & 0 \\ 0 & -m & 0 & m & m \end{bmatrix} \begin{bmatrix} \ddot{x}_1 \\ \ddot{y}_1 \\ \ddot{x}_2 \\ \ddot{y}_2 \\ \ddot{y} \end{bmatrix} + \begin{bmatrix} c_{1x} & 0 & 0 & 0 & -\mu c \\ 0 & c_{1y} & 0 & 0 & c \\ 0 & 0 & c_{2x} & 0 & \mu c \\ 0 & 0 & 0 & c_{2y} & -c \\ 0 & 0 & 0 & 0 & c \end{bmatrix} \begin{bmatrix} \dot{x}_1 \\ \dot{y}_1 \\ \dot{x}_2 \\ \dot{y}_2 \\ \dot{y} \end{bmatrix} + \begin{bmatrix} k_{1x} & 0 & 0 & 0 & -\mu k(t) \\ 0 & k_{1y} & 0 & 0 & k(t) \\ 0 & 0 & k_{2x} & 0 & \mu k(t) \\ 0 & 0 & 0 & k_{2y} & -k(t) \\ 0 & 0 & 0 & 0 & k(t) \end{bmatrix} \begin{bmatrix} x_1 \\ y_1 \\ x_2 \\ y_2 \\ f(y) \end{bmatrix} = \begin{bmatrix} 0 \\ 0 \\ 0 \\ 0 \\ F \end{bmatrix}. \quad (8)$$

Let $e(t) = e_a \cos(\omega t + \varphi_a) + e_b \cos(\omega t + \varphi_b)$,

$k(t) = k_m + k_a \cos(\omega t + \varphi)$, $\bar{k}_a = \dfrac{k_a}{k_m}$, $\xi_{44} = \dfrac{c_{2y}}{2m_2\omega_n}$, $\xi_{45} = \dfrac{c}{2m_2\omega_n}$, $\xi_{55} = \dfrac{c}{2m\omega_n}$,

$\overline{f(x_1)} = \bar{x}_1(t) = \dfrac{x_1(t)}{b}$, $\overline{f(y_1)} = \bar{y}_1(t) = \dfrac{y_1(t)}{b}$, $k_{11} = \dfrac{\omega_{1x}^2}{\omega_n^2}$, $k_{15} = \dfrac{\mu m}{m_1}$, $k_{22} = \dfrac{\omega_{1y}^2}{\omega_n^2}$, $k_{25} = \dfrac{m}{m_1}$,

$\overline{f(x_2)} = \bar{x}_2(t) = \dfrac{x_2(t)}{b}$, $\overline{f(y_2)} = \bar{y}_2(t) = \dfrac{y_2(t)}{b}$, $k_{33} = \dfrac{\omega_{2x}^2}{\omega_n^2}$, $k_{35} = \dfrac{\mu m}{m_2}$, $k_{44} = \dfrac{\omega_{2y}^2}{\omega_n^2}$, $k_{45} = \dfrac{m}{m_2}$,

$\bar{y}(t) = \dfrac{y(t)}{b}$, $\omega_{1x} = \sqrt{\dfrac{k_{1x}}{m_1}}$, $\omega_{1y} = \sqrt{\dfrac{k_{1y}}{m_1}}$, $\bar{t} = \omega_n t$, $k_{55} = 1 + \bar{k}_a \cos(\bar{\omega}\bar{t} + \phi)$, $\bar{\omega} = \dfrac{\omega}{\omega_n}$,

$\omega_{2x} = \sqrt{\dfrac{k_{2x}}{m_2}}$, $\omega_{2y} = \sqrt{\dfrac{k_{2y}}{m_2}}$, $\omega_n = \sqrt{\dfrac{k_m}{m}}$, $\bar{F}_m = \dfrac{F_m}{mb\omega_n^2}$, $\bar{F}_a = \dfrac{e_a}{b}(\bar{\omega})^2$, $\bar{F}_b = \dfrac{e_b}{b}(\bar{\omega})^2$,

$\xi_{11} = \dfrac{c_{1x}}{2m_1\omega_n}$, $\xi_{15} = \dfrac{\mu c}{2m_1\omega_n}$, $\xi_{22} = \dfrac{c_{1y}}{2m_1\omega_n}$, $\bar{F} = \bar{F}_m + \bar{F}_a \cos(\bar{\omega}\bar{t} + \varphi_a) + \bar{F}_b \cos(\bar{\omega}\bar{t} + \varphi_b)$,

$\xi_{25} = \dfrac{c}{2m_1\omega_n}$, $\xi_{33} = \dfrac{c_{2x}}{2m_2\omega_n}$, $\xi_{35} = \dfrac{\mu c}{2m_2\omega_n}$,

Dimensions normalized movement differential equations can be obtained as

$$\begin{bmatrix} 1 & 0 & 0 & 0 & 0 \\ 0 & 1 & 0 & 0 & 0 \\ 0 & 0 & 1 & 0 & 0 \\ 0 & 0 & 0 & 1 & 0 \\ 0 & -1 & 0 & 1 & 1 \end{bmatrix} \begin{bmatrix} \ddot{\bar{x}}_1(\bar{t}) \\ \ddot{\bar{y}}_1(\bar{t}) \\ \ddot{\bar{x}}_2(\bar{t}) \\ \ddot{\bar{y}}_2(\bar{t}) \\ \ddot{\bar{y}}(\bar{t}) \end{bmatrix} + 2 \begin{bmatrix} \xi_{11} & 0 & 0 & 0 & -\xi_{15} \\ 0 & \xi_{22} & 0 & 0 & \xi_{25} \\ 0 & 0 & \xi_{33} & 0 & \xi_{35} \\ 0 & 0 & 0 & \xi_{44} & -\xi_{45} \\ 0 & 0 & 0 & 0 & \xi_{55} \end{bmatrix} \begin{bmatrix} \dot{\bar{x}}_1(\bar{t}) \\ \dot{\bar{y}}_1(\bar{t}) \\ \dot{\bar{x}}_2(\bar{t}) \\ \dot{\bar{y}}_2(\bar{t}) \\ \dot{\bar{y}}(\bar{t}) \end{bmatrix} + \begin{bmatrix} k_{11} & 0 & 0 & 0 & -k_{15}k_{55} \\ 0 & k_{22} & 0 & 0 & k_{25}k_{55} \\ 0 & 0 & k_{33} & 0 & k_{35}k_{55} \\ 0 & 0 & 0 & k_{44} & -k_{45}k_{55} \\ 0 & 0 & 0 & 0 & k_{55} \end{bmatrix} \begin{bmatrix} \overline{f(x_1)} \\ \overline{f(y_1)} \\ \overline{f(x_2)} \\ \overline{f(y_2)} \\ \overline{f(y)} \end{bmatrix} = \begin{bmatrix} 0 \\ 0 \\ 0 \\ 0 \\ \bar{F} \end{bmatrix} \quad (9)$$

where,

$$\overline{f(y)} = \frac{f(y)}{b} = \begin{cases} \bar{y} - 1 & \bar{y} > 1, \\ 0 & -1 \le \bar{y} \le 1, \\ \bar{y} + 1 & \bar{y} < -1. \end{cases} \quad (10)$$

This model to simulate the gear transmission system has included the varying stiffness and the meshing impact in the gear meshing. The meshing impact part is relevant with the gear errors, time-varying stiffness, and the gaps.

3. The solution of the gear transmission nonlinear dynamics model

$$\begin{bmatrix}1&0&0&0&0\\0&1&0&0&0\\0&0&1&0&0\\0&0&0&1&0\\0&-1&0&1&1\end{bmatrix}\begin{bmatrix}\ddot{x}_1(t)\\\ddot{y}_1(t)\\\ddot{x}_2(t)\\\ddot{y}_2(t)\\\ddot{y}(t)\end{bmatrix}+2\begin{bmatrix}\xi_{11}&0&0&0&-\xi_{15}\\0&\xi_{22}&0&0&\xi_{25}\\0&0&\xi_{33}&0&\xi_{35}\\0&0&0&\xi_{44}&-\xi_{45}\\0&0&0&0&\xi_{55}\end{bmatrix}\begin{bmatrix}\dot{x}_1(t)\\\dot{y}_1(t)\\\dot{x}_2(t)\\\dot{y}_2(t)\\\dot{y}(t)\end{bmatrix}+\begin{bmatrix}k_{11}&0&0&0&-k_{15}k_{55}\\0&k_{22}&0&0&k_{25}k_{55}\\0&0&k_{33}&0&k_{35}k_{55}\\0&0&0&k_{44}&-k_{45}k_{55}\\0&0&0&0&k_{55}\end{bmatrix}\begin{bmatrix}f(x_1)\\f(y_1)\\f(x_2)\\f(y_2)\\f(y)\end{bmatrix}=\begin{bmatrix}0\\0\\0\\0\\F\end{bmatrix} \quad (11)$$

where,

$$f(y)=\begin{cases}y-1 & y>1,\\ 0 & -1\le y\le 1,\\ y+1 & y<-1.\end{cases} \quad (12)$$

Runge-Kutta numerical integral method is employed to solve the gear nonlinear dynamics differential equations. The five second-order differential equations in Eq. (11) are transferred to ten first-order differential equations first; Rounge-Kutta method will be used to solve these equations then. In order to realize the first step, a variable **q** has been introduced, as Eq. (13)

$$\begin{aligned}\mathbf{q}&=\{q_1,q_2,q_3,q_4,q_5,q_6,q_7,q_8,q_9,q_{10}\}^T\\&=\{x_1,\dot{x}_1,y_1,\dot{y}_1,x_2,\dot{x}_2,y_2,\dot{y}_2,y,\dot{y}\}^T,\end{aligned} \quad (13)$$

Then, Eq. (11) can be written in a new matrix form

$$\dot{\mathbf{q}}=\mathbf{H}\mathbf{q}+k_{55}f(q_9)\mathbf{A}+\mathbf{B} \quad (14)$$

where

H ——Linear coefficient matrix;

A ——Nonlinear coefficient vector;

B ——Load coefficient vector.

For writing convenience, the symbol "—" on the top of each of the variable in Eqs. (9) and (10) is removed as follows:

$$\mathbf{H}=\begin{bmatrix}0&1&0&0&0&0&0&0&0&0\\-k_{11}&-2\xi_{11}&0&0&0&0&0&0&0&\xi_{15}\\0&0&0&1&0&0&0&0&0&0\\0&0&-k_{22}&-2\xi_{22}&0&0&0&0&0&-\xi_{25}\\0&0&0&0&0&1&0&0&0&0\\0&0&0&0&-k_{33}&-2\xi_{33}&0&0&0&-\xi_{35}\\0&0&0&0&0&0&0&1&0&0\\0&0&0&0&0&0&-k_{44}&-2\xi_{44}&0&\xi_{45}\\0&0&0&0&0&0&0&0&0&1\\0&0&-k_{22}&-2\xi_{22}&0&0&k_{44}&2\xi_{44}&0&-\xi_{25}-\xi_{45}-2\xi_{55}\end{bmatrix},$$

$$\mathbf{A}=\{0\ \ k_{15}\ \ 0\ \ -k_{25}\ \ 0\ \ -k_{35}\ \ 0\ \ k_{45}\ \ 0\ \ -k_{25}-k_{45}-k_{55}\}^T,$$

$$\mathbf{B}=\{0\ \ 0\ \ 0\ \ 0\ \ 0\ \ 0\ \ 0\ \ 0\ \ 0\ \ F\}^T.$$

For Eq. (14), we can use the ode45( ) function in Matlab software of MathWorks Inc. to solve it. At the same time, we can carry out numerical simulation calculation using the Simulink toolbox of Matlab also.

4. The numerical simulation

The parameters of a gear transmission are show in Table 1. Z_1 and Z_2 are the teeth numbers of the gears. α and m are the pressure angle and the modulus of each of the gears, respectively. The meshing stiffness has been acquired with the coupled thermo-elastic contact finite element method [3]. The static error takes the reference of the experiment value of Munro [4], $e_a=20\mu m,\ e_b=3.45\mu m$.

Table 1. Gear parameters

Normal load (N/mm)	Z_1	Z_2	α	m (mm)
190	21	67	20º	2.5

4.1 The basic characteristics of the system

The time domain diagram, frequency domain diagram, phase plot, and Poincaré map of the system are shown in Fig. 2~6. The reciprocating aperiodic properties of the chaos vibration can be found in the phase plots. The phase traces of a period movement should be closed curves [5], while chaos does not have any periodicity. Therefore, the phase traces of the chaos vibration are not closed curves. Besides, the reciprocating property of the chaos vibration reflects that phase trace is limited in a bounded region. The phase trace cannot divergent to infinite distance. When the period of the period movement increase, it is hard to distinguish a period movement or a chaos according to the phase plots only. Poincaré map can depict the aperiodic property of a chaos better. If a Poincaré map is not a finite point set or a closed curve, then, the corresponding movement is a chaos probably.

In Fig.2, the rotation speed of the drive gear is equal to 3000 rpm, the systematic response is a simple-harmonic response. The time domain diagram is a standard sine wave; the phase plot is an ellipse; the Poincaré map is a single point; the frequency component appears at the exciting frequency only. This is identical to that of the linear system, namely, single frequency excitation, single frequency response. When the speed is equal to 3600 rpm, chaos has appeared, as Fig. 3. The time process is aperiodic. Phase plot is the locus that fills a certain part of the phase space. The locus is not repeated, not also closed. Poincaré map is not finite point set or a closed curve. The frequency domain diagram is some wide, attenuating gradually, and continuous in a limited frequency range. When the speed is equal to 4,199.15 rpm (Fig.4), response of the system is three-periodicity vibration. Poincaré map contains three dispersed points. The frequency domain diagram spreads at 1/3 of the harmonics of the fundamental frequency. When the speed is equal to 4799.53 rpm, the systematic response is two-period sub-harmonic response (Fig.5). The time durations are two-period movements, respectively. Poincaré map contains two dispersed points. The frequency components spread at 1/2 of the harmonics of the fundamental frequency. When the speed is equal to 9000 rpm (Fig.6), the systematic response is simple harmonic response. This shows that when the meshing frequency is far away from the natural frequency of a system, the response of the system tends to steady state again.

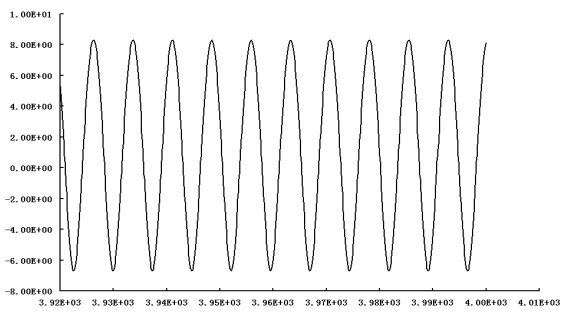

(a) Time domain diagram

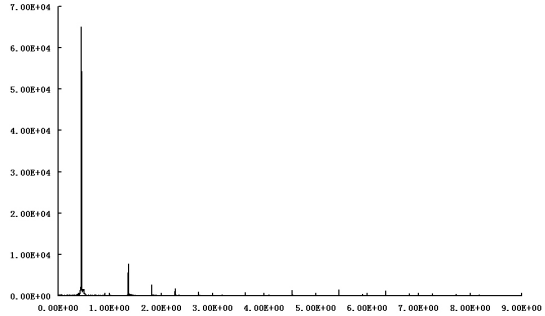

(b) Frequency domain diagram

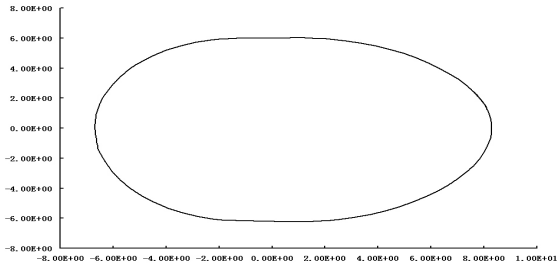

(c) Phase plot

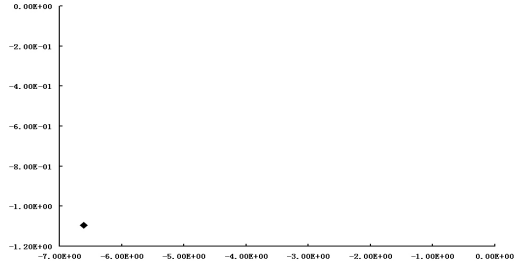

(d) Poincaré map

Fig. 2 The time domain diagram, frequency domain diagram, phase plot, and Poincaré maps when the rotation speed of the driven gear is 3000 rpm.

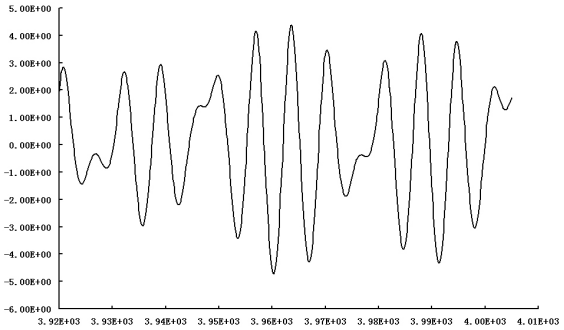

(a) Time domain diagram

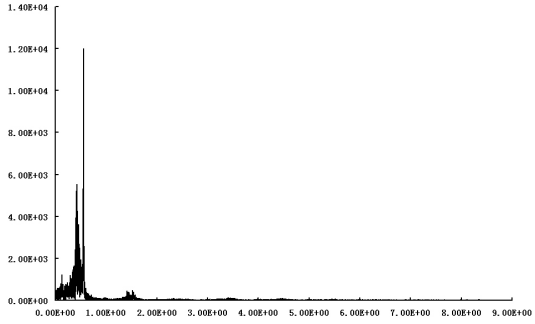

(b) Frequency domain diagram

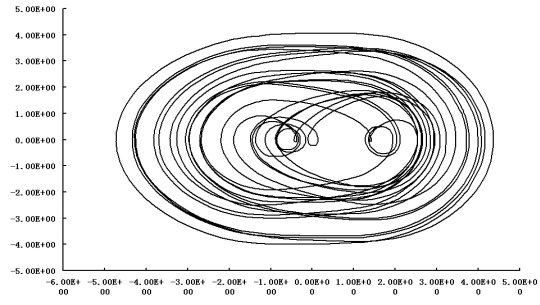

(c) Phase plot

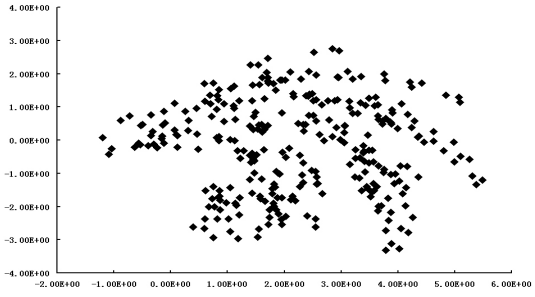

(d) Poincaré map

Fig. 3 The time domain diagram, frequency domain diagram, phase plot, and Poincaré maps when the rotation speed of the driven gear is 3600 rpm.

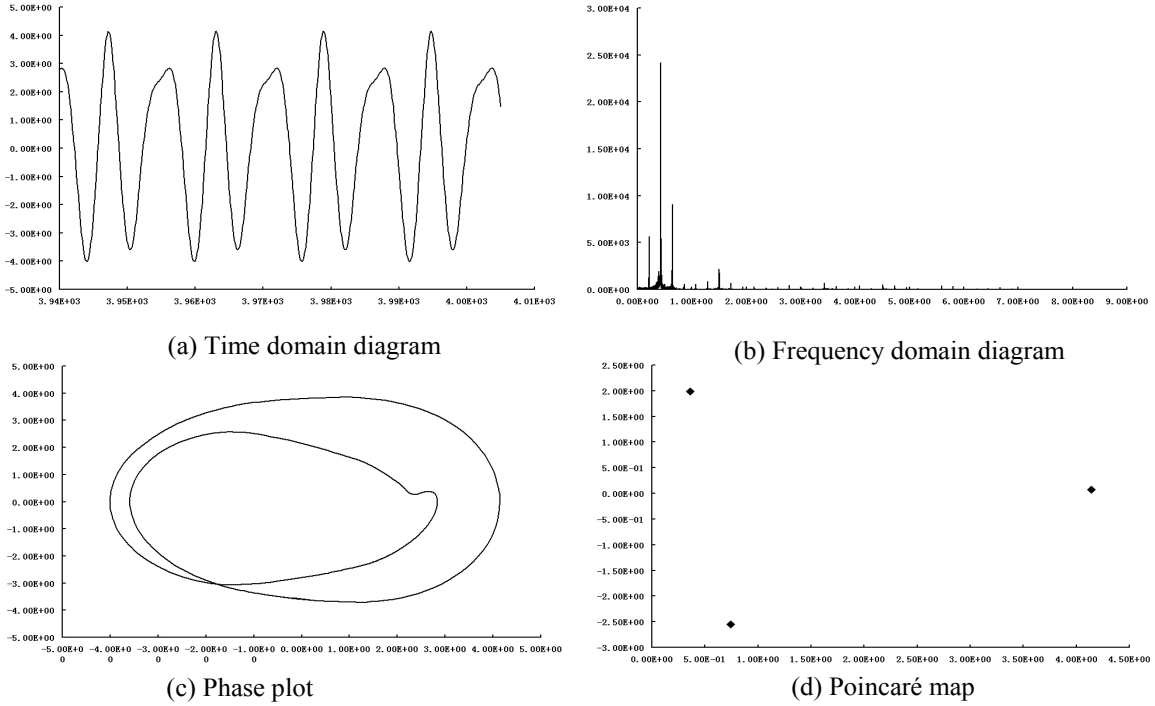

(a) Time domain diagram

(b) Frequency domain diagram

(c) Phase plot

(d) Poincaré map

Fig. 4 The time domain diagram, frequency domain diagram, phase plot, and Poincaré maps when the rotation speed of the driven gear is 4199.15 rpm.

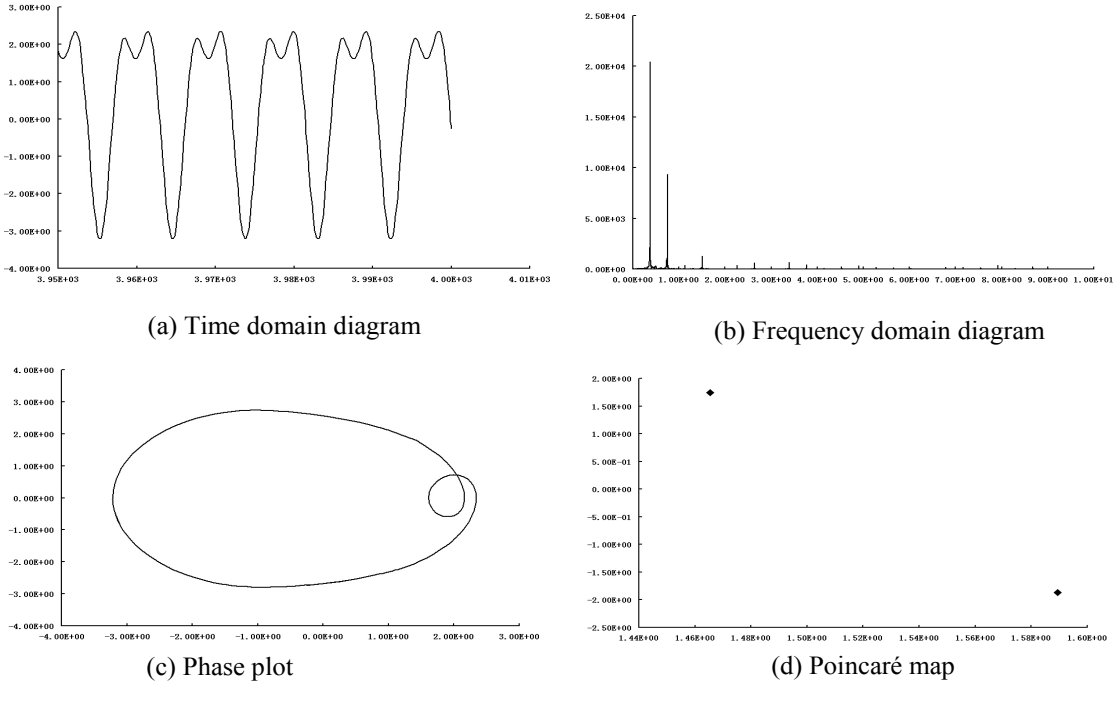

(a) Time domain diagram

(b) Frequency domain diagram

(c) Phase plot

(d) Poincaré map

Fig. 5 The time domain diagram, frequency domain diagram, phase plot, and Poincaré maps when the rotation speed of the driven gear is 4799.53 rpm.

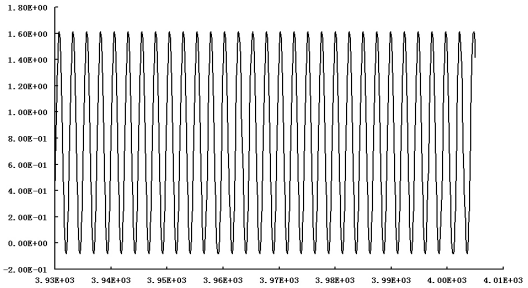

(a) Time domain diagram

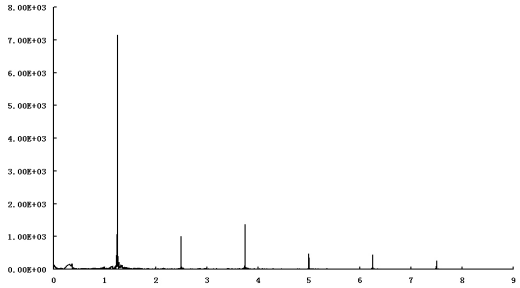

(b) Frequency domain diagram

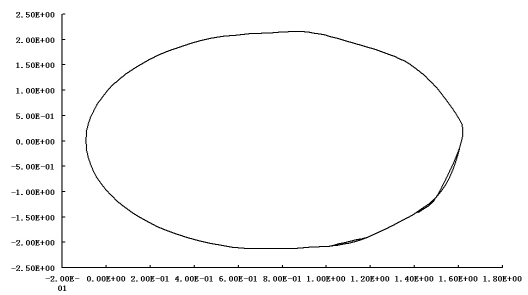

(c) Phase plot

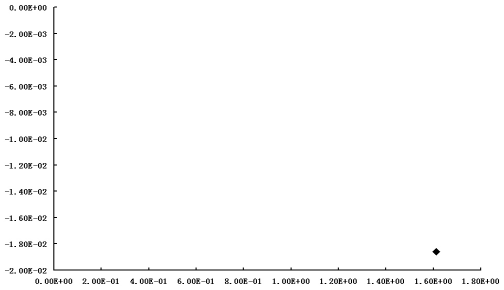

(d) Poincaré map

Fig. 6 The time domain diagram, frequency domain diagram, phase plot, and Poincaré maps when the rotation speed of the driven gear is 9000 rpm.

4.2 The systematic parameters' influences on the dynamic properties

4.2.1 The influence of time-varying stiffness

As former description, the time-varying meshing stiffness can be treated as a simple harmonic function. The proportion of the average amount and the varying amount of a meshing stiffness of a different gear pair is different. The fluctuation level of the time-varying stiffness, defined as a stiffness fluctuation factor c_ε, is described by the proportion of the varying amount k_a and the average amount k_m. That is $c_\varepsilon = k_a / k_m$. The following study presents the frequency response properties of the gear transmission system when c_ε=0, 0.2, and 0.4, respectively. In Fig.7, no matter the meshing stiffness is changing or not, the amplitude of every frequency response curve generated by meshing vibration increases considerably around the resonance frequency. With the increase of c_ε, the resonance frequency corresponding to the biggest amplitude becomes small and the vibration amplitude at the resonance frequency increases at the same time.

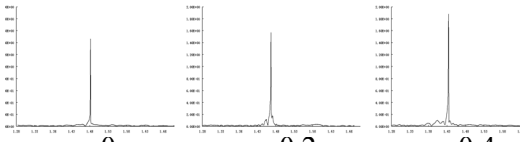

Fig. 7 Frequency response properties

4.2.2 The influence of gear errors

If neglecting the fluctuation of the load, the

exciting force generated by the load of system can be treated as the average excitation. The meshing error makes contributions to the changing excitation. Three frequency response properties of the gear transmission system are obtained when $\bar{e}$ = 0.2, 2, and 4, respectively. Where, $\bar{e}$ is the amplitude of the dimension error. In Fig.8, it can be found that the response amplitudes increase with the increase of the errors; the vibration of the gear transmission system will strengthen greatly.

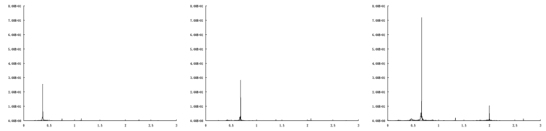

Fig. 8 Frequency response properties

4.2.3 The influence of the gaps on the aperiodic property of chaos

The influence generated by the gaps can be represented in the time, frequency, and phase domain. This section only discusses the influence on the phase plot. The calculation results are shown in Fig.9 when *b*=20, 125, and 127 μm, respectively.

In Fig.9, the gaps have little influence on the aperiodic property in a certain scope. But, with the increase of the gaps, the system vibration has moved from a single frequency response towards chaos state quickly, and the meshing impact has been aggravated.

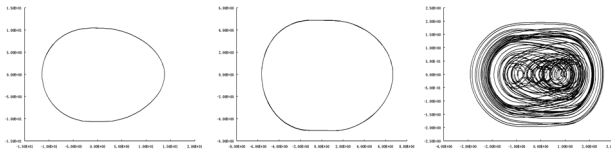

Fig.9 Phase plots at different gaps

5. Conclusion

A dynamics model is developed, in which the time-varying gear meshing stiffness, errors, and gap are considered. The model is solved by numerical methods in Matlab environment. The calculation results are represented by the time domain diagram, frequency domain diagram, phase plot, and Poincaré map. The system response rules are obtained based on these diagrams. Therefore, we can estimate a system's dynamic properties in the design process and make the system avoid resonance frequency as far as possible. At last, this paper has analyzed the influence of the system parameters' change on the dynamic properties and reached some beneficial conclusions.

References

[1] Runfang Li, Jianjun Wang. Gear system dynamics. Beijing: Science Press, 1997.

[2] Hongbin Yang, Xiaozhong Deng, Jianping Gao, and Zhongde Fang. The summary of gear nonlinear vibration research. China Mechanical Engineering, 1999, 10(7): 807~809.

[3] Shaobin Li, Runfang Li, and Tengjiao Lin. Cylindrical gear teeth ideal modification curve based on the coupled thermo-elastic contact finite element method. China Mechanical Engineering, 2003, 14(7), 1175~1179.

[4] R. G. Munro. The dynamic behavior of spur gears. Cambridge University, 1962, Ph. D. Dissertation.

[5] Yanzhu Liu, Liqun Chen. Nonlinear vibration. Beijing: Higher Educational Press, 2001.

Shaobin Li received the Dr. Eng. degree from Chongqing Univ. in 2004. He has been an associate professor at Chongqing Normal Univ. since 2002. His research interest includes CAD/CAE/CAM, and their application to engineering.

Hong-Zhong Huang is a professor at School of Mechatronics Engineering, University of Electronic Science and Technology of China (He is currently a Visiting Professor of Department of Mechanical Engineering, Northwestern University, 2145 Sheridan Road, Evanston, IL 60208-3111, USA)